Super-Resolution for Line Parallel Imaging in Energy Dispersive X-Ray Diffraction

Ferréol Soulez, Charles Crespy, Valerie Kaftandjian, Philippe Duvauchelle, Angela Peterzol, Pascal Ponard

Spatial super-resolution for line parallel imaging in energy dispersive X-ray diffraction

Ferréol Soulez[1], Charles Crespy[1], Valerie Kaftandjian[1], Phillippe Duvauchelle[1], Angela Peterzol[1], Pascal Ponard[2]
[1]CNDRI (Nondestructive Testing using Ionizing Radiation) Laboratory, INSA-Lyon, 25 Av. Jean Capelle 69621 Villeurbanne cedex, France
[2]Thales Components Subsystems, 2 rue Marcel Dassault 78941 Vélizy cedex

Abstract

We present a proof of concept for a new approach for Energy Dispersive X Ray Diffraction (EDXRD) imaging in "line parallel" configuration. It follows an inverse problem approach using a physical model of the diffraction phenomenon. Using this approach, we show that it is possible to achieve a spatial super-resolution of poly-crystalline objects (i.e. estimating more voxels than detectors).

1 Introduction

EDXRD is used to provide information about crystalline structure of material. It consists in measuring coherent photons scattered by a sample at a fixed angle. The sample is irradiated by a polychromatic X ray pencil beam. The spectrum obtained is linked to the atomic planar spacing of the sample according to the Bragg law and thus can be used for materials identification.

X Ray Diffraction Imaging (XRDI) is a modality where measurements are made in many volume elements (voxels) of the studied object. For practical use of this technique in security screening [5], acquisition speed is a critical requirement. As pointed out in [6], each single acquisition is time consuming, and thus, designing massively parallel acquisition scheme is a necessity. One of the simplest technical solution for such scheme is the "line-parallel" XRDI defined in [6] and illustrated by the figure 1.

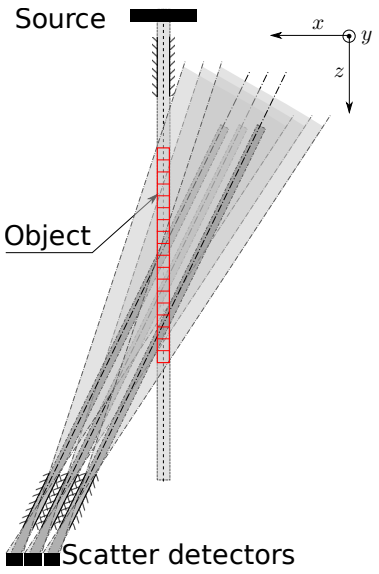

Figure 1: *Schematic view of the setup and notations used in the model.*

In this paper, we present a method for data processing in line-parallel XRDI. In this framework, a line of scatter detectors provides diffraction profiles of parts

of the object at different depths along the irradiation beam. Using the fact that areas observed by each scatter detectors overlapped, we propose method which enhances spatial resolution of this line-parallel XRDI. Following an inverse problems approach, this method uses a physical model to estimate the interference functions in each and every voxels of the studied sample. It thus provides a super-resolution of the interference function map where there is more voxels than detectors.

2 Direct Model

The EDXRD setup is composed of a collimated poly-chromatic X-ray source and a collimated spectroscopic detector D placed at angle θ from the beam axis. The studied object O is placed at the center of the diffractometer defined as the intersection of the scatter collimator axis and the source collimator axis.

To define our direct model, we consider an elementary surface of one detector $\mathrm{d}\boldsymbol{d}$, an elementary surface of the source $\mathrm{d}\boldsymbol{s}$ and an elementary volume of the object $\mathrm{d}\boldsymbol{o}$. This triplet define the scattering angle θ. In the case the studied sample is a crystal, the average number of photons $m(\lambda)$ arriving at each energy, on the detector $\mathrm{d}\boldsymbol{d}$ is given by crystallographic theory (see [2, 4]):

$$m(E) = \frac{r_e^2\,(h\,c)^3}{16\,\pi\,E^3}\,N(E)\,A(E)\,L(\theta)\,G(\mathrm{d}\boldsymbol{s},\mathrm{d}\boldsymbol{o},\mathrm{d}\boldsymbol{d})\,f(x)\,, \tag{1}$$

where :

- $N(E)$ is the number of photons emitted by the source at energy E,
- $A(E)$ is the attenuation of the object at energy E,
- $L(\theta)$ is the Lorentz factor,
- $G(\mathrm{d}\boldsymbol{s},\mathrm{d}\boldsymbol{o},\mathrm{d}\boldsymbol{d})$ is a geometrical factor accounting for the effects of collimators and of the distance between source object and detectors,
- $f(x)$ is the interference function of the studied sample. It is expressed in momentum transfer $x = \frac{E}{h\,c}\sin\left(\frac{\theta}{2}\right)$. It depends on the form factor, the volume of the crystal cell, the multiplicity, the texture of the considered crystal.

This last term $f(x)$ is the function we wish to estimate for material identification.

Integrating this function over whole source, object and detectors, we are able, after discretization, to build an operator $\mathbf{H}$ that models the diffraction in our setup :

$$\boldsymbol{m} = \mathbf{B}\cdot(\mathbf{H}\cdot\boldsymbol{f})\,, \tag{2}$$

where :

- $\mathbf{B}$ is the spectral response of detectors,
- $\boldsymbol{m}$ is the modeled measurements vector of size $N_E \times N_D$ with N_E the number of energy channel and N_D the number of detectors,
- $\boldsymbol{f}$ is the interference function map of size $N_x \times N_V$ with N_x the number of estimated momentum transfer channel and N_V is the number of voxels.

Finally, during the aquisition by the detector data are corrupted by photon counting noise $\boldsymbol{n}$ which follows a Poisson law.

2.1 Model validation

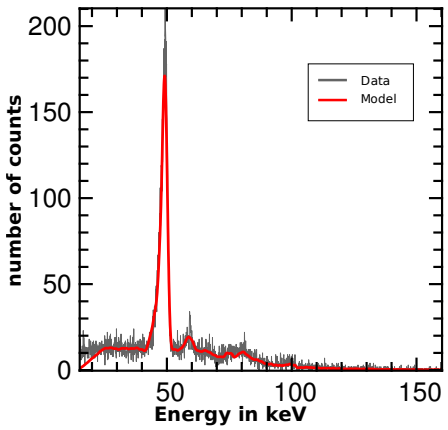

Figure 2: *Scattering measurements on a Graphite sample (in gray) and their modeling (in red) using the model defined by equation 2. An automatically estimated continuous background, accounting non modeled effects (multiple and Compton scattering) was added to fit these data.*

We have validated this direct model using experimental measurements of known material. In figure 2, we present, for one detector, the experimental scattering measurements of a piece of graphite. The setup used was the same that the one used for simulation and described in section 4.1. These data can be compared with their model in red. As we can see, our model fits quite well the measurements proving the effectiveness of our model.

3 The inverse problems approach

We aim to retrieve the interference function map $\boldsymbol{f}$ using the measurements $\boldsymbol{y}$ (of size $N_E \times N_D$). In an inverse problem approach (see [9]), we estimate theses unknowns that best reproduce the measurements $\boldsymbol{y}$ according to the direct model defined by equation 2. As there is more unknowns than data, this problem is ill-posed and we propose to resolve it in a maximum a posteriori (MAP) framework by defining some priors about these unknowns. These prior will be injected in the problem by some regularization functions. The main issue about priors definition was the fact that pure amorphous (e.g. liquids) and pure crystalline materials present very different diffraction profiles. To bypass this problem, we defined two maps, one for crystalline, the other for amorphous materials such as $\boldsymbol{f} = \boldsymbol{f}_{\text{cryst}} + \boldsymbol{f}_{\text{amorph}}$. Different priors are then defined for $\boldsymbol{f}$, $\boldsymbol{f}_{\text{cryst}}$ and $\boldsymbol{f}_{\text{amorph}}$:

- Interference function of crystal is almost null everywhere except on values verifying the Bragg law. Corresponding regularization function $\phi_{\text{cryst}}(\boldsymbol{f}_{\text{cryst}})$ is a ℓ_1 norm designed to enforce sparsity [3].
- Interference function of amorphous materials is smooth in the momentum

transfer space. Corresponding regularization function $\phi_{\text{amorph}}(\boldsymbol{f}_{\text{amorph}})$ is simple quadratic smoothing regularization function.

- Along the depth dimension, in an additional spatial prior, we suppose that if there is a change of materials between two adjacent voxels, the interference function will change radically. $\phi_{\text{spatial}}(\boldsymbol{f})$ is a vector valued TV regularization function [8].
- in addition, force the estimated maps $\boldsymbol{f}_{\text{cryst}}$ and $\boldsymbol{f}_{\text{amorph}}$ to be positive.

Finally, the estimated map $\boldsymbol{f}^{\text{MAP}}$ is the solution that minimizes a cost function $\phi_{\text{cost}}(\boldsymbol{f})$. This function is composed of a likelihood function $\phi_{\text{ML}}(\boldsymbol{f})$ ensuring the agreement between the model and the data plus the *a priori* functions (regularization functions) $\phi_{\text{cryst}}(\boldsymbol{f})$, $\phi_{\text{amorph}}(\boldsymbol{f})$ and $\phi_{\text{spatial}}(\boldsymbol{f})$:

$$\boldsymbol{f}^{\text{MAP}} = \arg\min_{\boldsymbol{f}} \left[\phi_{\text{ML}}(\boldsymbol{f}) + \alpha\,\phi_{\text{cryst}}(\boldsymbol{f}_{\text{cryst}}) + \beta\,\phi_{\text{amorph}}(\boldsymbol{f}_{\text{amorph}}) + \gamma\,\phi_{\text{spatial}}(\boldsymbol{f})\right], \tag{3}$$

where α, β and γ are three tuning hyper-parameters which are used to balance the influence of both *priors* and likelihood and that have to be properly tuned. The minimization is made using a limited memory continuous optimization method (L-BFGS [7]).

4 Simulation

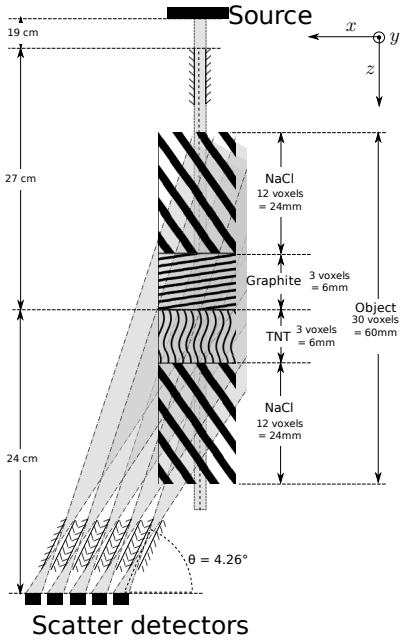

Figure 3: *Schematic view of the setup used for our simulation.*

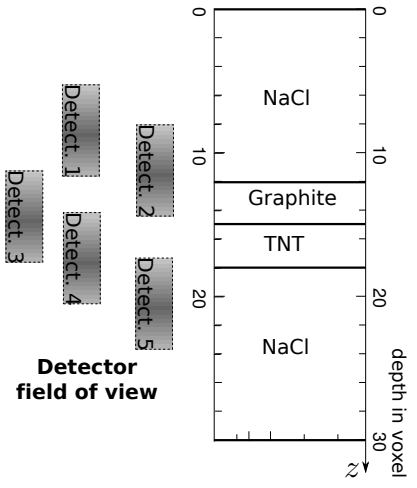

Figure 4: *Composition of the simulated sample and field of view of each detector.*

This method was then tested on several realistic simulated data with three or four components. We present here a result in simulation with only crystalline materials.

4.1 Simulated setup

The setup dimension are described by the figure 3. The sample is irradiated by a 140 kV X-ray tube with a tungsten anode. We consider that the X-ray spectrum follows the Birch and Marshall empirical spectrum [1]. The diameter of the focal spot is 1 mm. The incident X-ray beam is collimated with a slit of 0.2 mm in width, 8 mm in height and 8 cm in length. The scattered photons are detected with an line of five detectors oriented at $\theta = 4.26$ degree. The collimators located in front of each detectors have a slit of 0.02 mm in width, 8 mm in height and 8 cm length. The resolution in energy of each detector is fwhm = 0.9 keV and is supposed to be constant on the whole energy range considered in these experiments. With such a couple source/detector, we consider energies between 15 keV and 160 keV. This corresponds to 1818 energy channels of the detector.

4.2 Data simulation

The sample was composed of a line 30 voxels of size $2 \times 2 \times 2$ mm along the X ray beam axis (depth). The sample is composed of three crystalline powders. As illustrated on figure 3, following the z axis, we dispose first 12 voxels of NaCl, 3 voxels of graphite, 3 voxels of TNT and finally 12 more voxels of NaCl. This disposition corresponds to the $\boldsymbol{f}$ vectors which is presented on figure 4. The figure shows momentum transfer versus voxels indices. The four different areas of the figure correspond to the four components. As all the materials are crystalline, bright line at momentum transfer position corresponding to crystal inter-planar spacing can be seen on the figure. Figure 4 presents also the field of view of each detector which is about 6 voxels. The total volume "seen" by our setup is about 20 voxels. In this configuration, we simulated measurements using our direct model using theoretical attenuation of such object. To process more realistic simulated data, we added a continuous background. These simulated data were then corrupted by photon noise. These data are presented on figure 5.

All these spectra exhibit several peaks above a continuous background. As the field of view of each detector is quite wide (cf. Fig. 4), these peaks may be due to different materials. For example, the spectrum of the third detector exhibits peaks caused by TNT and graphite and the spectrum of the fourth detector exhibits peaks caused by TNT and NaCl.

5 Results and discussion

The data were processed by our algorithm. The estimated map of the crystalline component of interference functions $\boldsymbol{f}_{\text{cryst}}^{\text{MAP}}$ is presented on figure 6 and can be compared with the map $\boldsymbol{f}$ used for the simulation shown on figure 7. As we can see, the algorithm effectively estimate interference functions in each observed voxel. For example, in the voxels 4 to 12 and 18 to 24, the three main peaks of NaCl are correctly placed at 1.8, 2.5 and 3.08 nm^{-1}. Due to the energy range of the detector, the interference functions were not estimated

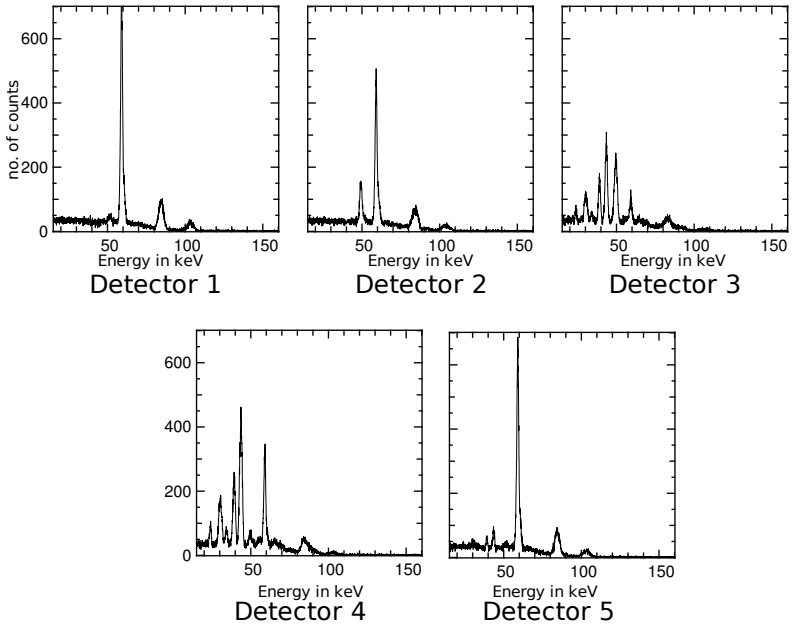

Figure 5: *Scattering measurements on the five detectors.*

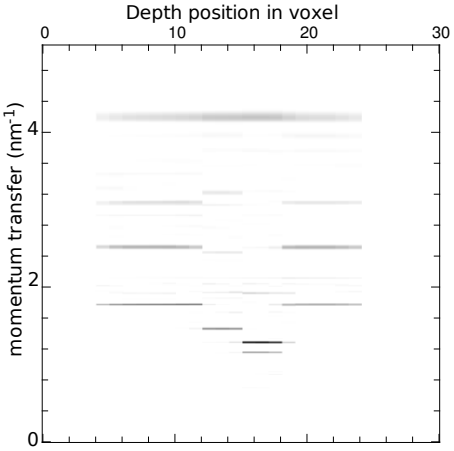

Figure 6: *Crystalline component of estimated interference function map* $\boldsymbol{f}_{\text{cryst}}^{\text{MAP}}$ *by processing data presented in figure 5.*

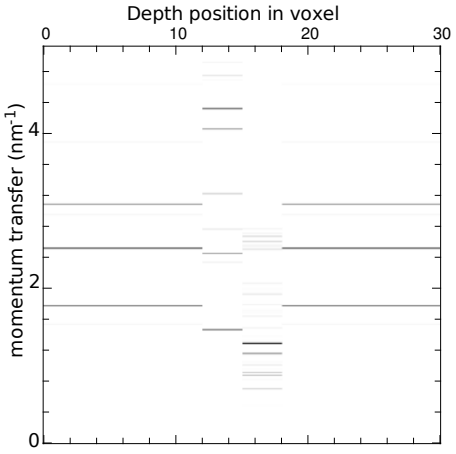

Figure 7: *Theoretical interference function map* $\boldsymbol{f}$ *used in the simulation. It shows momentum transfer in function of the voxel position is depth (z). The darker is a pixel, higher is the interference function at corresponding voxel and momentum transfer.*

for momentum transfer below than $1\,\text{nm}^{-1}$ and higher than $4.5\,\text{nm}^{-1}$. The interference functions of voxels before 4 and after 24 are zero as these voxel are out of the field of view of our setup.

As our purpose is to estimate powder diffraction diagram of the crystalline

parts for material identification we do not show the amorphous component of estimated map. In reality the amorphous component $\boldsymbol{f}_{\text{amorph}}$ does not only account for amorphous parts of the sample but for continuous background too. Indeed, a continuum in the data can be view by our model as a continuum in the momentum transfer space. Thus, as our goal was only to estimate crystalline component, this formulation, even if it have no physical meaning, can be used to explain continuum.

Moreover, the separation between each materials which was difficult to assess by a simple observation of the data is now obvious. In some case, the interference function of one voxel may spread to the next voxel. This happens when an interference function peak is very low or when the number of photons measured at corresponding energy is close to zero. This is particularly the case for the graphite peak at $4.1\,\text{nm}^{-1}$ ($137\,\text{keV}$ at $\theta = 4.26°$) which spreads on almost all observed voxels.

As a conclusion, these results demonstrate the super-resolution capability of our method. Indeed, we effectively estimate interferences functions in twenty voxels with only five scatter detectors, improving thus the resolution by a factor of four.

To process the simulation, we supposed that we know the attenuation and the source spectrum. This is usually not the case in reality. One solution is to place a spectrally resolved detector in transmission that may give a good estimation of the product of the source spectrum by the attenuation. However, preliminary results show that even a very coarse approximation of the spectrum and the attenuation affect only the magnitude but not the position of peaks.

Acknowledgements

The authors gratefully acknowledge the support of the French National Research Agency (ANR), under grant SPIDERS (ANR-AAP-07-CSOSG) and all the consortium members.

References

[1] R. Birch and M. Marshall. Computation of bremsstrahlung x-ray spectra and comparison with spectra measured with a ge (li) detector. *Physics in Medicine and Biology*, 24:505–517, 1979.

[2] M. Birkholz, P.F. Fewster, and C. Genzel. *Thin film analysis by X-ray scattering*. Vch Verlagsgesellschaft Mbh, 2006.

[3] D.L. Donoho. Compressed sensing. *Information Theory, IEEE Transactions on*, 52(4):1289–1306, 2006.

[4] A. Guinier. *Theorie et Technique de la Radiocristallographie*. Dunod, 2 edition, 1956.

[5] G. Harding. X-ray scatter tomography for explosives detection. *Radiation Physics and Chemistry*, 71(3-4):869–881, 2004.

[6] G. Harding. X-ray diffraction imaging—a multi-generational perspective. *Applied Radiation and Isotopes*, 67(2):287–295, 2009.

[7] Jorge Nocedal. Theory of algorithms for unconstrained optimization. *Acta Numerica*, 1:199–242, 1992.

[8] G. Sapiro and DL Ringach. Anisotropic diffusion of multivalued images with applications tocolor filtering. *IEEE Transactions on Image Processing*, 5(11):1582–1586, 1996.

[9] A. Tarantola. *Inverse Problem Theory and Methods for Model Parameter Estimation*. Society for Industrial Mathematics, 2005.